Constant Parameter Three Dimensional Finite Element Model for Structural Concrete

Salek M. Seraj

Widespread usage of the finite element method in the analysis of reinforced concrete members designed in accordance with the currently prevalent ultimate limit state philosophy is largely precluded by the notorious lack of generality of the finite element models for structural concrete. Such shortcomings as regards applicability to arbitrary structural components are usually combined with the need to deal with several material input parameters, some of which are not readily obtainable and/or need to be varied with problem type. Nevertheless, the recent development of a fully three-dimensional finite element model, based on a brittle constitutive relationship at the material level, appears to be capable of reliable predictions irrespective of structural type, even though the material properties (i.e. both the constitutive relations and the failure criteria) are reduced to the specification of the most basic parameter, namely the cylinder strength of concrete, the assessment of which is both straightforward and reliable. Recently, various case studies on plain-, reinforced- and prestressed-concrete (PC, RC, PSC) members having varying complexities and made from both normal- and high-strength concrete (NSC, HSC) have been conducted to test this model. The present paper summarises these finding in an effort to show that the "constant parameter" finite element model, as well as serving as a tool for analysis, can also provide insight into limit state design itself.

THE FINITE ELEMENT MODEL

Various features, objectivity, generality, applicability and performance of the presently discussed "constant parameter" non-linear finite element

Bangladesh University of Engineering & Technology, Dhaka, Bangladesh

model have recently formed the basis of a number of publications of Gonzalez Vidosa et al. (1991a, 1991b, 1991c) and Seraj et al. (1992a, 1992b). A forthcoming publication of Kotsovos and Pavlovic (1995) encompasses a comprehensive treatment of the present model.

Characteristics of the Finite Elements Used

The 20-node serendipity element HX20 was chosen for modelling concrete and a 3-node parabolic element LM03 (with axial stiffness only) was adopted for modelling reinforcing bars. The finite elements used are shown in Fig. 1. Both of them are isoparametric with parabolic shape functions and, hence, they can adjust to non-straight boundaries.

The numerical integration of brick element HX20 was carried out by means of the 2x2x2 Gaussian-integration rule. Similarly, for element LM03, integration was done at 2 Gauss points. Although the whole topic of the order integration is one undergoing much current discussion, the latest contributions by the proposers of the presently adopted FE model (Gonzalez Vidosa et al. 1988, 1991a) seem to suggest that the favourable effect of under-integration of the 3-D isoparametric element in linear problems appears to hold also for the constant parameter nonlinear structural concrete FE model presently described.

It should be noted that in the present modelling of concrete structures, the steel elements must coincide with the edges of the serendipity element, because the HX20 element cannot allow a more flexible distribution of steel bars due to the absence of mid-face and centre nodes when compared to the Lagrangian element.

Fig. 1 Selected 3-D finite elements: (a) HX20, 20-node serendipity element (concrete) and (b) LM03, 3-node uniaxial element (steel)

Constitutive Relations and Failure Criteria

The constitutive relations for monotonically increasing short-term loading are the result of purely experimental data for a wide range of uniaxial, biaxial and triaxial tests (Kotsovos and Newman 1979). The ensuing equations are, in essence, curves of best fit to all these data and, typically, they take the form depicted in Fig. 2. Several important features exhibited by such characteristics are worth mentioning. First, all relations are uniquely defined upon the specification of the cylinder strength in uniaxial compression, f_c. Secondly, the characteristics consist exclusively of ascending branches, i.e. concrete is a fully brittle medium at the material level (Kotsovos 1984). While the absence of any descending branch in compression has been proved experimentally (Kotsovos 1983),

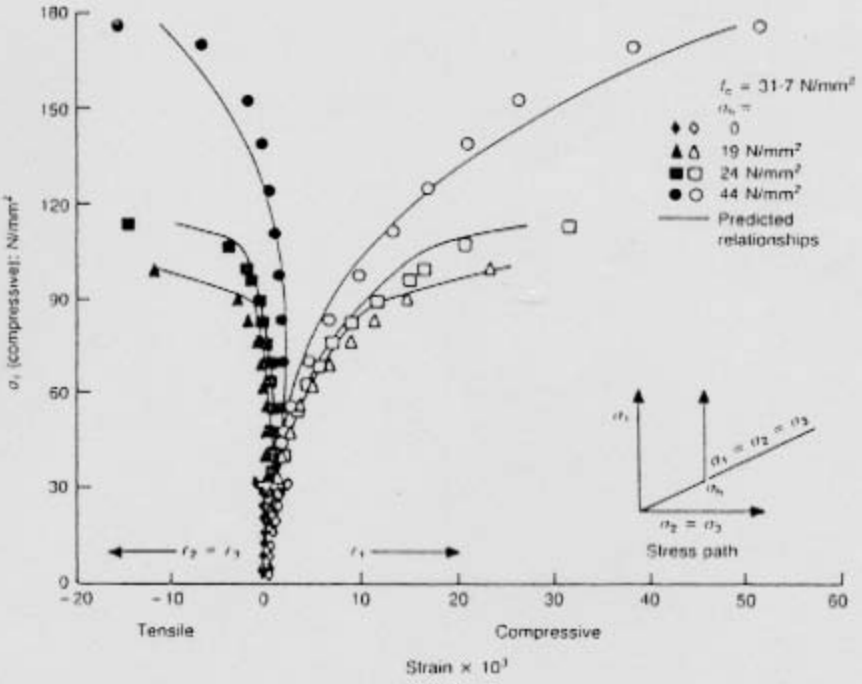

Fig. 2 Stress-strain relationship for a typical concrete strength (f_c=31.7 MPa) under a given stress path (after Kotsovos and Pavlovic, 1986)

it has been shown by Gonzalez Vidosa et al. (1991b) that, even the inclusion of any hypothetical "strain-softening" relations in the analysis would make no difference to the predictions. Thirdly, the presence of triaxial effects (such as the hydrostatic-stress level σ_h in Fig. 2) is sufficient to cause large increases in strains before failure, thus indicating that the brittle nature of concrete is perfectly compatible with the observed ductile behaviour of many concrete structures (Kotsovos 1982). Fourthly, the extremely rapid increase in lateral expansion of a concrete specimen as the peak compressive stress is approached should be noticed (see ε_2, ε_3 in Fig. 2) since this plays a key role on the mode of failure of structural concrete members (Gonzalez Vidosa et al. 1991b).

The mathematical description of the strength envelope of concrete under arbitrary combinations of stress is also based on a close fit of most uniaxial, biaxial and triaxial experimental strength data available, and, as before, is fixed upon the sole specification of f_c (Kotsovos 1979). A 3-D view of the predicted failure surface appears in Fig. 3. Perhaps the most important feature of the strength envelope is the very significant effect of even small secondary stresses superimposed on the principal stress component. Their effect is to substantially increase or decrease the ultimate strength value depending on whether they are compressive or tensile in nature, respectively.

The trilinear characteristics adopted for portraying the material description of the reinforcing steel is shown in Fig. 4. Diagram A relates to cold-drawn steels, whereas diagram B applies to mild steels. Note that the first two branches are completely defined once Young's Modulus and f_y are specified, while the third branch requires the specification of the stress and strain at failure (Gonzalez Vidosa et al. 1991a). Although a bilinear diagram might be more appropriate for mild steels, it is convenient to predict earlier yielding of the steel so as to avoid uncertainties associated with possible sudden yielding in the last non-converged load step of the analysis, thus being able to differentiate clearly between ductile and brittle behaviours.

In Fig. 5, the stress-strain relationship of a typical prestressing strand has been shown diagrammatically. Due to the absence of a real yield stress value in a prestressing tendon, a stress equivalent to 1% strain has been conveniently chosen as the yield stress, f_y. If f_u is considered as the ultimate stress of the tendon, and σ_p as the stress up to which the tendon is stressed after all the losses have taken place, it is sensible to use the values of $(f_y-\sigma_p)$ and $(f_u-\sigma_p)$ as inputs of $f_{y,model}$ and $f_{u,model}$, respectively. Thus, by removing the part of the stress-strain curve utilised during the prestressing operation from the actual stress-strain curve of the tendon, and by using this modified stress-strain curve as input in the FE model, the effects of the prestressing force in the tendon can be represented

without the more formal inclusion of initial stresses and strains (Seraj et al. 1992b).

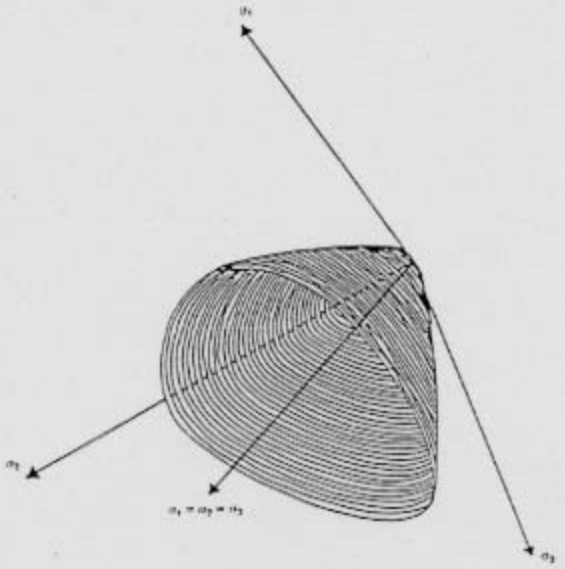

Fig. 3 Three-dimensional view of the predicted ultimate strength surface (after Kotsovos, 1979)

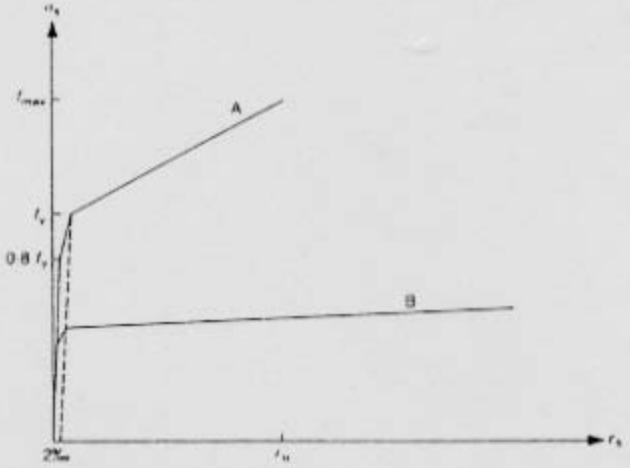

Fig. 4 Stress-strain diagram for steel: high-yield steel A and mild Steel, B (after Gonzales Vidosa et al., 1991a)

Other Material Parameters

When concrete cracks, there is a reduction in shear moduli across the plane of the crack, and it is usual to define these by multiplying their uncracked values by the shear retention factor (henceforth SRF), β (<1). This factor is clearly associated with the notion of "aggregate interlock", widely regarded as contributing significantly to the shear resistance of cracked regions. However, a proper interpretation of experimental evidence shows the opposite conclusion to be correct since the reproduction of such evidence through numerical modelling was achieved by adopting a very small value of SRF (Kotsovos and Pavlovic 1986). Thus, the view that aggregate interlock plays a negligible role in the load-carrying capacity of a member is reflected in the present analysis by the adoption of a value of SRF of 0.1.

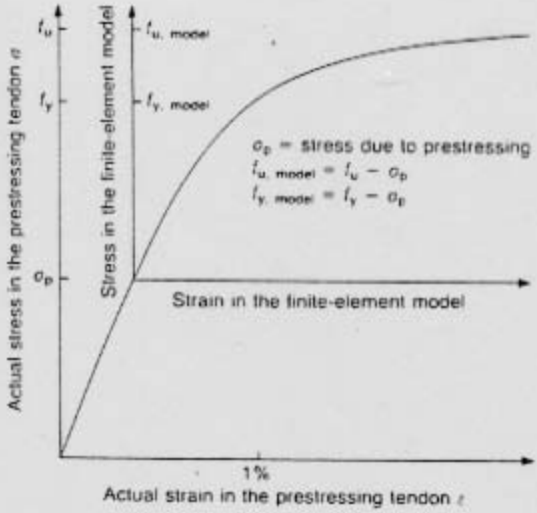

Fig. 5 Stress-strain diagram for prestressing tendon (after Seraj et al., 1992b)

Three factors ought to be considered in modelling those regions of the structure where reinforcement is located. The first of these concerns the so-called "dowel action" of the bars themselves. Here, the sole stiffness component along the axis of the reinforcement is compatible with the view that the effect of the dowel action is insignificant (Kotsovos et al., 1987). The second factor is the question of the bond between steel bars and surrounding concrete. Since the nodes of the steel element coincide, throughout the analysis, with the nodes of the corresponding concrete element edges, the perfect-bond assumption is implicit. Kotsovos and Pavlovic (1986) have argued that such a stand-point is consistent with the use of the "smeared crack" approach (adopted in the present model) which spreads the effect of cracking over a region that may far exceed the localised region where bond-slip occurs, thus precluding a detailed modelling of the steel-concrete interaction. Moreover, the limited data available on bond-slip stress magnitudes suggests that tensile cracking in the concrete will have occurred prior to any bond-slip (Kotsovos and Pavlovic, 1986).

Finally, there is the tension-stiffening factor which aims to account for the fact that, despite the appearance of cracks orthogonal and adjacent to steel bars, there is stiffness in the uncracked portions of the concrete between cracks, and hence some residual average stiffness in the concrete additional to that of the steel alone. This effect is not considered in the present model which, in accordance with the smeared crack philosophy, assumes all the material in the region of the cracks to have lost its stiffness. Such a simplification also keeps the mesh pattern reasonably simple, as it does not require cracks in the concrete elements to be distinguished depending on whether they occur around reinforcement or in plain concrete regions. Nevertheless, it is expected that ignoring the tension-stiffening effect might have some bearing on the accuracy of computed deformations, by underestimating the stiffness of the relevant parts of the structure, as discussed elsewhere (Gonzalez Vidosa et al., 1991a). It should be mentioned that the notion of tension-stiffening which, strictly speaking, refers to cracked concrete adjacent to steel (i.e. RC ties), is partly responsible for the assumption of strain-softening for concrete in tension irrespective of its location with respect to steel. On the other hand, the present model adopts perfectly-brittle stress-strain characteristics for concrete in tension, as was the case for compression, as outlined earlier.

Smeared Modelling of Cracking

The straightforward and manageable "smeared cracking" (Rashid, 1968) method, which distributes the cracks throughout a finite region, is

adopted in the present model. This approach consists of modifying the constitutive matrices (which, prior to cracking, are isotropic and hence identical in any set of axes) for those zones of the structure in which the triaxial combination of stresses (including, invariably, at least one tensile component) exceeds the failure envelope, thus incorporating the loss of rigidity stemming from microcracking into the gradually degrading structure stiffness matrix. Such stiffness loss also implies stress modifications that lead to residual forces that are necessary to preserve equilibrium. As in most versions of smeared modelling, the present approach simulates cracking by modifying the constitutive matrices and stresses at those Gauss points where the failure envelope has been attained, hence enabling the numerical integration of the stiffness matrices and the calculation of the residual stresses to proceed.

The constitutive (or D-) matrices which are adopted for cracked Gauss points are compatible with the notion of brittleness at the material level discussed earlier. When the ultimate-strength envelope at a Gauss point is exceeded for the first time (in tension or tension-compression combinations), a cracked plane is formed perpendicular to the direction of the maximum tensile stress existing prior to cracking. Such tensile stress is set to zero and transformed into unbalanced forces to be distributed throughout the surrounding zones. The value of β is set to 0.1 to avoid excessive deterioration of the stiffness matrix, with possible ill conditioning. If the state of stress at a given Gauss point reaches the triaxial envelope in tension a second time, then a second crack plane is assumed to form. Such a new crack plane is orthogonal to the current maximum tensile principal stress and, consequently, is not necessarily orthogonal to the first crack plane. The combination of the two crack planes only leaves stiffness in the direction of the intersection of both planes (direction 2' or AB in Fig. 6). As for the one-crack case, some residual shear stiffness has to be kept in order to improve the conditioning of the cracked stiffness matrices. If the state of stress reaches the failure envelope for a third time (again, invariably, in tension) two options have been considered. The first option is to use a zero constitutive matrix (i.e. complete loss of stiffness in all directions), and the second - to be used in the present work - is to adopt a matrix with only residual values of βG (the latter option arises, again, from the same reasons as for the one- and the two-crack cases), G being the shear rigidity.

Incremental Procedure Adopted

The iterative method chosen for the nonlinear analysis is the well-known incremental Newton-Raphson technique (Zienkiewicz, 1977). Gonzalez Vidosa et al. (1991a) introduced a strategy which can achieve

both computational economy and numerical stability by updating all (constitutive) D-matrices at the first iteration of each load step and then only updating the D-matrices pertaining to the two sources of high localised (i.e. "strong") nonlinearities (cracking of concrete and yielding of steel) as soon as these nonlinearities occur. This strategy of selective updating was referred to as the NR-plus method and has been adopted in the present model.

Since the cracking in the brittle model tends to produce large residual forces, the number of cracks allowed to form in a given iteration must be controlled in order to avoid numerical instabilities (Gonzalez Vidosa et al., 1988). Two extreme strategies were used in the past (Kotsovos and Pavlovic, 1986), the "total-crack approach" (TCA), which allowed all prospective cracks to occur at once, and the "single-crack approach" (SCA), with allowance of the most critical crack only. Gonzalez Vidosa et al. (1988) pointed out that for finite load steps, these two strategies often result in considerably different predictions and recommended the adoption of SCA as a generally more stable strategy. It should be pointed out that the term SCA has been used in a somewhat more general sense, thus denoting those cases where cracks are allowed to occur in small pre-determined numbers. In all the analyses of this study, up to two new cracks per iteration has been used.

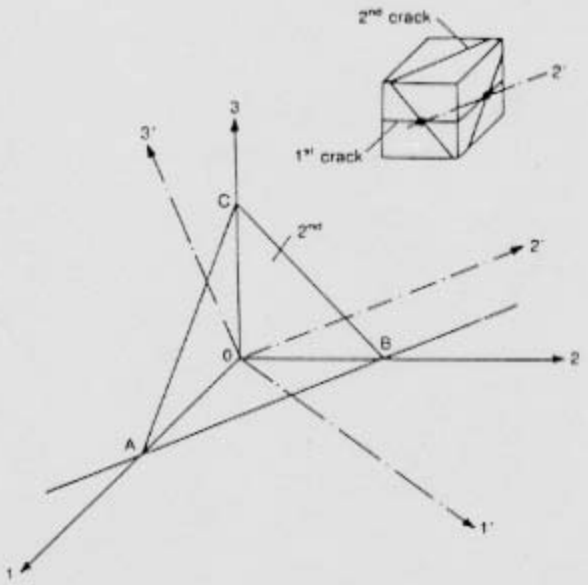

Fig. 6 Local axes for a one- and two-crack Gauss point (after Gonzalez Vidosa et al., 1991a)

Plotting Convention

As regards plotting convention, plots are superimposed onto the mesh lying on a plane parallel to the reference plane (XZ). The symbols for the various cracks at the relevant Gauss points are as follows. Oriented dashes represent the intersection of a crack plane with the plotting plane XZ whenever the angle subtended between these two planes exceeds 45°. Should both planes form an angle smaller than 45°, the crack plane is indicated by a circle. Three cracks at the same Gauss point are indicated by an asterisk. Displacement shapes at the various load levels can be suitably magnified, and the appearance of very large and/or distorted shapes helps to identify quickly the onset of a mechanism (whether real or numerical in nature); the latter is especially relevant for load step "777" plots that relate to the last performed iteration in an analysis. Finally, it should be remembered that, in all instances, the maximum sustained load (MSL) is taken to represent failure, even though the MSL corresponds to the last converged load step. Load step "777" (corresponding to the MSL plus an additional load-step increment), if shown, is for reference only.

CASE STUDY 1: PC PRISM UNDER STRIP LOADING

The details of the FE mesh (comprising 4 brick elements) adopted by Gonzalez Vidosa et al. (1991a) in studying the plain-concrete prism tested by Niyogi (1974) is shown in Fig. 7. The figure also contains analytical crack patterns at first cracking and ultimate loads. In the actual test, the PC prism was subjected to concentric strip loads (f_c = 26.9 MPa, ultimate bearing stress = 17.4 MPa). As in the experiments, the crack patterns show that vertical cracks develop in the inner zone of the prism (under the strip load), with accompanying horizontal cracks in the outer zone resulting from differential vertical deformations of these two regions. In the present case study, the maximum sustained Load (MSL) of 19 MPa was about 9% above the experimental failure load (EXP) of 17.4 MPa.

CASE STUDY 2: PSC I-BEAM CW12 FAILING IN WEB SHEAR

The structural element under examination is a pretensioned PSC beam having an I-section, reinforced with both prestressing and non-prestressing reinforcing bars, and reported as CW12 by Elzanaty et al. (1985). The cross-sectional characteristics and transverse reinforcement details of the beam are given in Fig. 8. The prestressing reinforcement was made up of 4-0.6 in (15 mm) diameter low-relaxation seven-wire

ASTM Grade 270 strands. The area of each wire was 0.22 in^2 (141.93 mm^2). The stress at 1% extension was 253.55 ksi (1748.67 MPa) and the ultimate stress was 268.09 ksi (1848.95 MPa). Two types of non-prestressing reinforcing bars were used: deformed ASTM Grade 60, having an actual yield stress of 63 ksi (434 MPa) for the longitudinal reinforcement and stirrups of 3/8 in (9.5 mm) diameter; and smooth round bars of 0.25 in (6.3 mm) diameter, having a yield stress of 55 ksi (379 MPa), for the top reinforcement. The concrete cylinder strength for this beam was 5800 psi (40 MPa) while it was prestressed by an effective prestressing force of 96.8 kip (430.56 kN). Due to the small web thickness, single-legged stirrups at 10 in (254 mm) spacing were used. The portion of such reinforcement in the flange was arranged alternately, as can be seen from Fig. 8. The beam was loaded by two-point loading with a shear span to depth ratio, a/d, equal to 3.75. The loads for the onset of diagonal cracking and ultimate failure for this beam were 170.8 kN and 281.1 kN, respectively.

The details of the FE mesh are shown in Fig. 9. The mesh comprises 50 brick elements for the concrete and 192 bar elements for the steel. Figure 9 also indicates the area of reinforcement of the various steel elements of the mesh. The prestressing and non-prestressing steel elements were treated separately. The former were "smeared" to the adjoining brick element edges in such a manner that the point of application of the resultant prestressing force remained unchanged. The effective prestressing stress, σ_p, was equal to 758.38 MPa. After subtracting the value of σ_p from the stress-strain curve of the tendon, the $f_{y,model}$ and $f_{u,model}$ for the FE input were found to be equal to 990.29 MPa and 1090.57 MPa, respectively. The non-prestressing steel area was also "smeared" to its adjacent nodes in a similar manner. The compression reinforcement was placed at the top edge of the beam and was discontinued in the flexural span. The main modification introduced in the modelling of the shear reinforcement was that the original one-legged alternately-placed stirrups were replaced by equivalent two-legged stirrups to introduce symmetry across the longitudinal direction; however, the total area of steel per unit length (both in the web and flanges) was kept the same as in the actual beam.

The prestressing force was applied at the end of the beam as a constant force acting on the outside nodes of the prestressing steel elements. The amount of prestressing force at different nodes was varied depending upon the area of the prestressing steel, so as to have everywhere the resultant prestressing force of the right magnitude and position. The vertical point loads were placed considering a/d to be equal to 3.75.

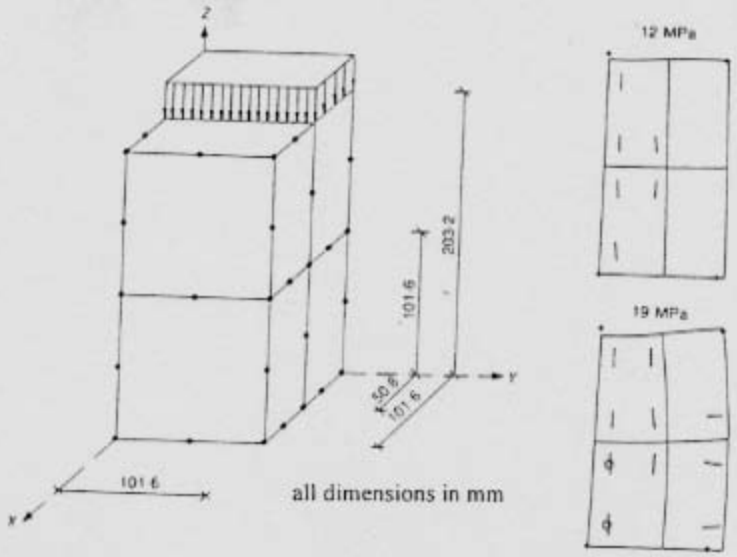

Fig. 7 Case study 1. FE mesh for one-eighth of the structure and analytical crack patterns (after Gonzalez Vidosa et al., 1991a)

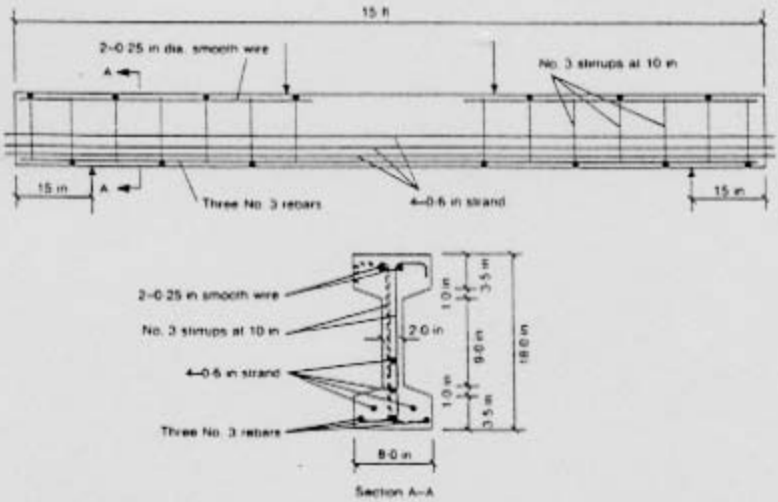

Fig. 8 Case study 2. Dimensions and reinforcement detailing (after Elzanaty et al., 1985)

The maximum sustained load in the analysis was 323.38 kN, which is 15% higher than the experimental failure load of 281.11 kN. The analytical results may be discussed with reference to Fig. 10, where the analytical crack patterns up to failure and a comparison of the analytical and experimental load-deflection curves have been shown. At the first load step, in which the effective prestressing force was applied to the beam all at once, cracks appeared at the end block of the beam parallel to the direction of the prestressing force. The beam remained free from any flexural or shear cracks up to a load of 182.78 kN when, suddenly, web-shear cracks emerged along the whole length of the shear span. These cracks, which were formed at all the Gauss points of the web elements (making an angle of about 22.5° with the longitudinal direction of the beam), resembled quite well the cracks that formed during the experiment, at the diagonal-cracking load of 170.8 kN. At a total applied load of 210.9 kN, the first flexural cracks appeared in the middle of the flexural span and, also, just below the point load. One of the shear cracks extended towards the support at this stage. With the increase in load, flexural cracks were also formed in the shear span. At 309.3 kN, cracks near the loading points in the shear span started to propagate into the flange (hitherto uncracked) towards the actual point loads. At the maximum sustained load (MSL), additional cracks were formed in the top flange, defining more completely the compressive force trajectory. At this load step, a vertical crack (indicated by a circle) in the top flange near the point load was visible.

As can be seen from Fig. 10, the analytical load-deflection curve practically coincides with its experimental counterpart up to the experimental failure load, and then continues to follow a tangential path up to the MSL. This increased load sustainment in the analysis can be explained with reference to the modelling of the stirrups. In order to keep the computational efforts within the limit of available resources, symmetrical stirrups had to be introduced. In doing so, even though the total amount of reinforcement was carefully kept equal to the quantity used in the test, an additional confinement of the concrete was introduced in the analysis. It is important to note that even a small amount of confining pressure (of the order of 0.1 f_c) is sufficient to increase the load-carrying capacity of concrete by more than 50% (Kotsovos and Newman 1981). It is, therefore, sensible to assume that, due to the introduction of additional confinement in the FE analysis of CW12, the concrete in the compression zone sustained more load and, in turn, led the structural element to a higher failure load. Load step "777" of Fig. 10 supports this view regarding the confinement, as it shows that concrete in the top flange underwent a considerable amount of dilation at failure. In the test, due to the presence of one-legged asymmetric stirrups, concrete (and thus the structural member) failed earlier as concrete in the

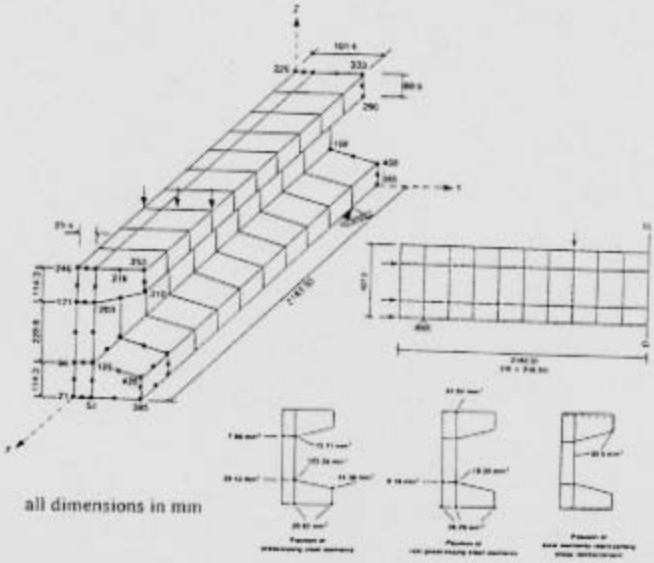

Fig. 9 Case study 2. FE mesh for one-fourth of the structure

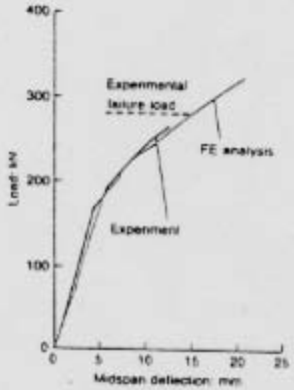

Fig. 10 Case study 2. Analytical crack patterns and comparison between experimental and analytical load-deflection curves

compression zone was not sufficiently confined. An additional reason for the numerical overestimate of the failure load is that the model used in the analysis relies greatly on the material properties. It should be stressed here that, in the input of the cylinder strength in the present FE analysis, the f_c value of the cylinder having the size 6x12 inch was used instead of the f_c value of the 100x250 mm (4x10 inch) cylinder required for the FE model. Now, Neville (1981) reported that, for an increase in the height/diameter ratio from 2 to 2.5, the cylinder strength value of normal-strength concrete can decrease by about 10%. This reduction in f_c, if allowed for in the input of the FE model, would certainly have closed the gap between the analytical and experimental failure loads for the present case study. (A re-run with an f_c value of 36 MPa (=0.9 of the f_c value of 100x250 mm cylinder) has, in fact, yielded a MSL of 309.32 kN, i.e. only 10% above the experimental failure load.) It is, thus, evident from the analysis of case study 2, that even after adopting a crude and simplistic way of modelling the effects of prestressing (and reinforcement detailing) within the 3-D FE package, a satisfactory and realistic response can be achieved in the numerical simulation of PSC structural forms.

CASE STUDY 3: PSC T-BEAM PCB6 FAILING IN FLEXURE

The cross-sectional characteristics and transverse reinforcement of the PSC T-beam PCB6 is shown in Fig. 11. The beam was subjected to six-point loading. The relevant experimental and design details of PCB6, prestressed to an effective prestressing force of about 60% and designed in compliance with the compressive-force path (CFP) concept is available elsewhere in Seraj et al. (1993a, 1993b). The f_c value for PCB6 was 45.7 MPa.

The FE discretization adopted for the analysis of PCB6 consists of 54 brick elements and 169 bar elements. Part of the mesh details is shown in Fig. 12. The longitudinal and transverse reinforcement was smeared to the edges of appropriate elements. The shape of the bottom flange has been slightly modified (essentially a reduction in area) in the FE discretization and should have minimal effect as per Seraj et al. (1992a).

The analytical crack patterns at different load levels up to failure appear in Fig. 13. The figure also contains comparison of analytical and experimental load-deflection curves. The MSL predicted by the analysis was 84.17 kN, which was about 92% of the total load sustained by the beam in the experiment. The steel end plate of the beam was properly modelled and, accordingly, the end zone remained free from longitudinal cracks. At 60.12 kN, the first set of flexural cracks appeared within the flexural span and below the inner load points. In the

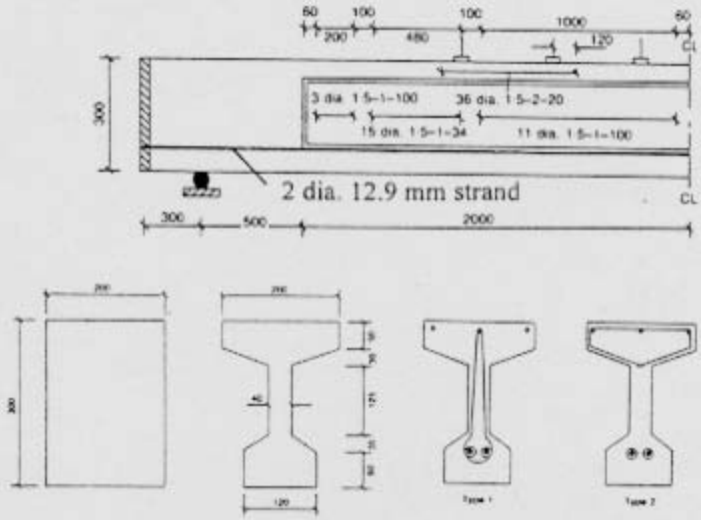

Fig. 11 Case study 3. Dimensions and reinforcement detailing

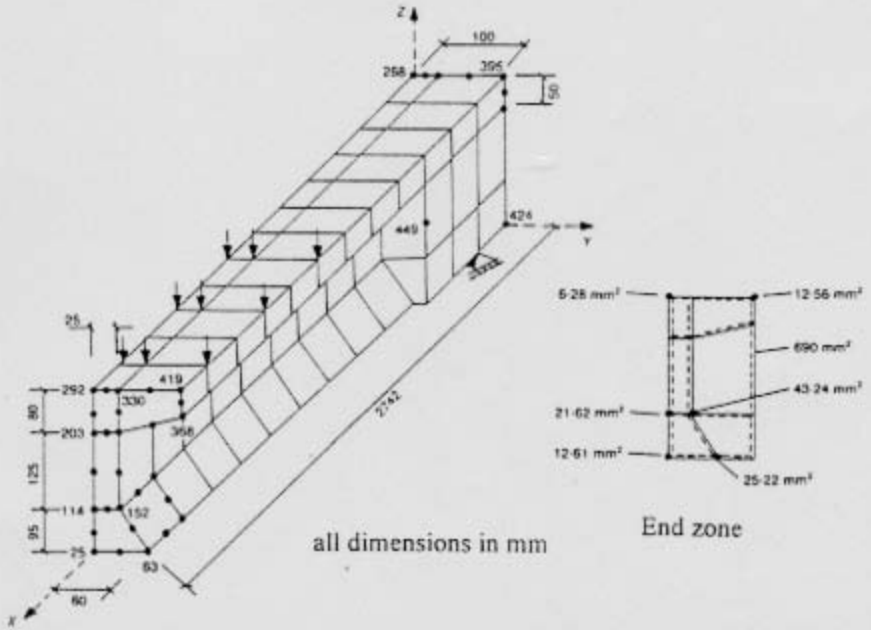

Fig. 12 Case study 3. FE mesh for one-fourth of the structure

subsequent load step, the number of flexural cracks increased. At a load of 72.14 kN, diagonal cracks, oriented from the supports to the point loads, developed throughout the web of the beam, while the central flexural cracks propagated upwards and reached the intersection of the web and the flange. In the following load step, the number of both flexural and shear cracks grew. Upon reaching the MSL level, the extension within the top flange of one of the flexural cracks of the flexural span could be seen, and the stress in the prestressing steel at the midspan of the beam passed the yield limit of the tendon. Inspection of the crack pattern at load step "777" reveals that, at failure, some of the flexural cracks in the midspan were greatly widened, as the material at the Gauss points corresponding to those concrete elements collapsed (i.e. third cracking) in the FE analysis.

The close agreement between experiment and analysis is also apparent from Fig. 13. The nature of both the experimental and the analytical curves points to a flexural failure of the beam; the actual ductility being adequately monitored in the analysis. Therefore, it is clear from the above analytical exercise that the load-carrying capacity, the cracking process and the deformational response of the PSC beam PCB6 have been closely simulated by the adopted FE model.

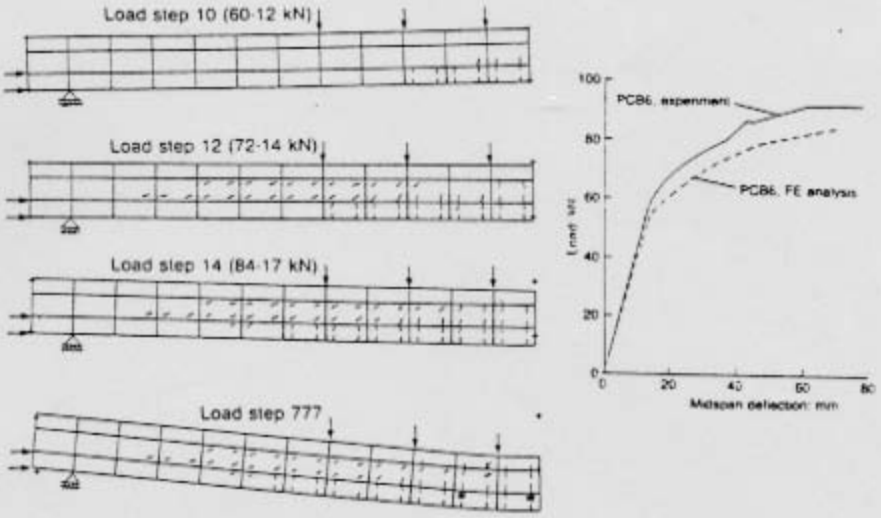

Fig. 13 Case study 3. Analytical crack patterns and comparison between experimental and analytical load-deflection curve

CASE STUDY 4: HSC BEAM B150-11-3 FAILING IN SHEAR

The structural element under study is a RC beam of rectangular cross-section, made from high-strength concrete and reported as B150-11-3 by Mphonde and Frantz (1984). The experimental details of the beam and the typical crack patterns at failure are given in Fig. 14. The yield strength of 1 inch (25 mm) diameter tension reinforcement and 1/8 inch and 3/16 inch (3.2 and 4.8 mm) diameter shear reinforcement was 448 MPa, 303 MPa and 269 MPa, respectively. The concrete strength was determined by testing 3x6 inch (76x152 mm) test cylinders. The equivalent standard 6x12 inch (152x305 mm) cylinder strength, assumed to be 92% of the smaller cylinder strength, was reported to be equal to 10080 psi (69.5 MPa). The average cross-sectional shear stresses at cracking and failure were 255 and 515 psi (1.76 and 3.55 MPa), respectively. From these reported values, the loads corresponding to cracking and ultimate failure were estimated to be equal to 160 and 323 kN respectively. The beam failed in "shear compression".

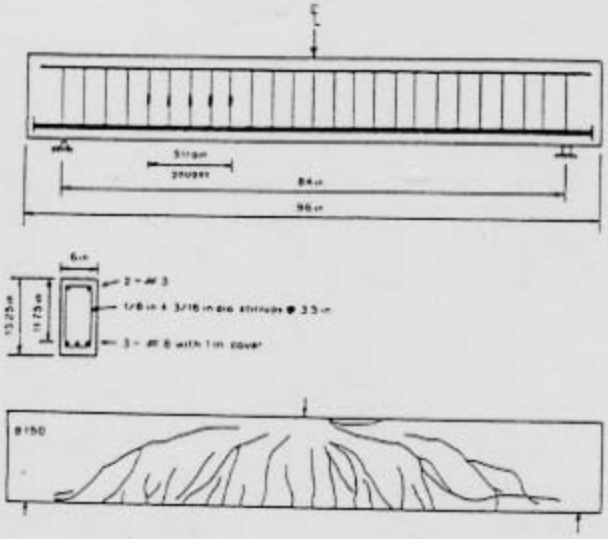

Fig. 14 Case study 4. Dimensions and reinforcement detailing and typical crack pattern at experimental failure (after Mphonde et al., 1984)

Figure 15 shows the FE discretization adopted for the present analysis. The mesh has 24 brick elements for the concrete and 64 bar elements for the steel (with reference to the one-fourth of the beam that was analysed). The reinforcement area for the various steel elements of the mesh is also indicated in Fig. 15. The tension reinforcement was concentrated at a distance from the top face equal to the effective depth of the beam and the concrete cover was neglected altogether; in this respect, the adopted mesh is compatible with the minor contribution of the cracked areas to the transfer of shear forces (Kotsovos et al. 1987), and, thus, it appears that neglecting the cover can only affect the deformational response of the beam, while the ultimate-load prediction is insensitive to such a simplification. The compression reinforcement was "smeared" to the top edge of the beam; again this modification is unlikely to affect results. While the spacing of the stirrups in the test was 88.9 mm, that in the model was 152.4 mm; thus the area of transverse reinforcement had to be adjusted so as to have the same stirrup shear capacity. Although both 303 and 269 MPa yield-strength stirrups were used in the test at the same location, only the 269 MPa stirrups were adopted for the analysis, in order to minimise the number of bar elements; however, the overall stirrup shear capacity was kept at the required value.

The MSL in the analysis was 360 kN, which is 11% above the experimental failure load. Figure 16 shows the analytical crack patterns at various load steps up to failure. At 72 kN, the first vertical flexural cracks were observed in the middle part of the beam. At the MSL of 360 kN, the extension of the more severe crack from the top surface of the beam towards the support through the compression zone of the beam is detectable through the new cracks formed under the load and at the support. Eventually, "shear" failure took place. The analytical crack pattern at the MSL (load step 20 in Fig. 16) resembles well its experimental counterpart (Fig. 16b). Stresses in both the longitudinal and transverse steel were below their yield limits at failure (i.e. load step 20). Figure 14 also includes the relevant load-deflection curves. It may be seen that both the experimental characteristic and the analytical prediction are in excellent agreement up to about 200 kN. However, beyond this load, the latter becomes stiffer. Now, the model used in the analysis relies greatly on the material properties. In this respect, it has already been pointed out that, in the absence of actual values of standard cylinder compressive strength, the value of f_c was estimated from 76.2x152.4 mm cylinder strengths. But such an estimated f_c reported by Mphonde and Frantz (1984) is applicable to the standard cylinder having size 6x12 inch. On the other hand, the input for f_c used in the FE model is based on the cylinder having size 100x250 mm (4x10 inches). Now, it

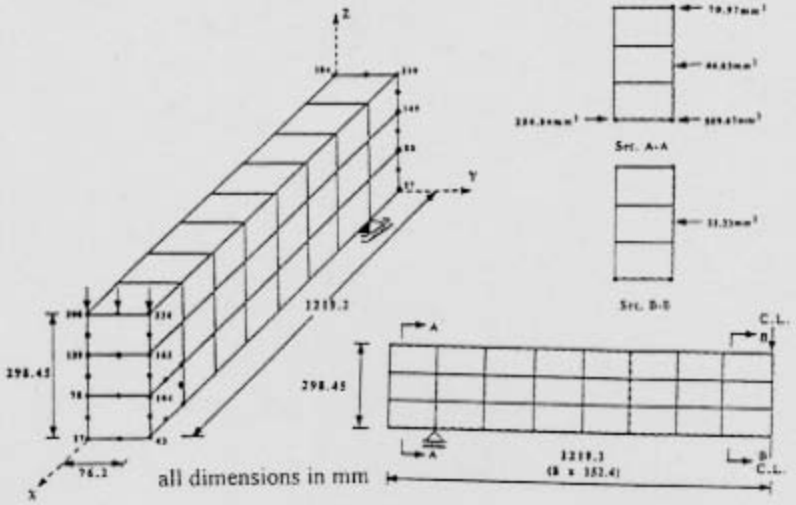

Fig. 15 Case study 4. FE mesh for one-fourth of the structure

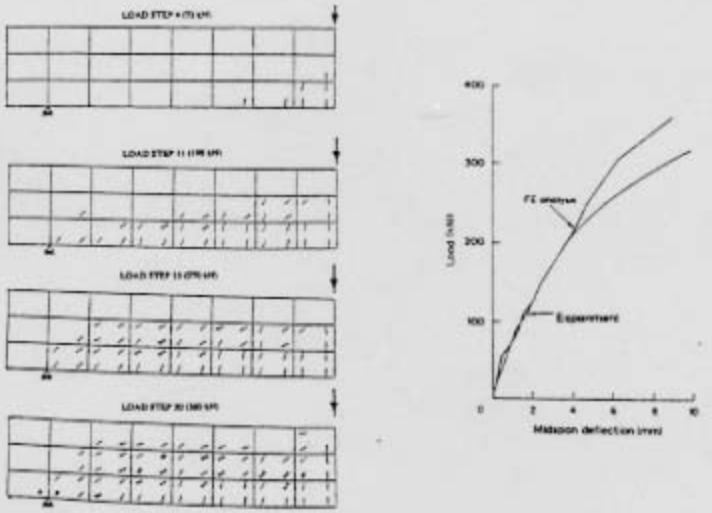

Fig. 16 Case study 4. Analytical crack patterns and comparison between experimental and analytical load-deflection curves

is known that, for an increase in the height/diameter ratio from 2 to 2.5, the f_c value of normal-strength concrete can decrease by about 10% (Neville, 1981). This reduction in f_c, although less pronounced in high-strength concrete, if considered in the input of the FE model, would have certainly closed the gap between the analytical and experimental failure loads for this case study. Also, the actual stress-strain curve of the reinforcing steel was not available; hence, the ultimate strength was assumed to be 15% higher than the yield strength. Nevertheless, despite these uncertainties, it appears that the present model simulates quite well the overall behaviour of a structural element with rectangular cross-section made from high-strength concrete.

CASE STUDY 5: HSC T-BEAM HSB2 FAILING IN FLEXURE

The size and sectional characteristics and reinforcement characteristics of the high-strength concrete member HSB2 is given in Fig. 17. The experimental and design details of beam HSB2, designed in accordance to the CFP concept, is available elsewhere (Seraj et al., 1994). The member was made from a concrete having a cube strength of 80 MPa (f_c=64 MPa). Details of the mesh (consisting of 25 brick and 74 bar elements) and the position and amount of the steel are given in Fig. 18. The longitudinal and transverse steel had to be "smeared" to its adjoining nodes in a manner similar to the earlier analyses. In the analysis, the flexural span was 1040 mm instead of 1000 mm; nevertheless, this deviation is of minor consequence. In the analysis of HSB2, the yield stress and the ultimate stress of the 6 mm ϕ transverse reinforcement were taken as 570 MPa and 665 MPa, respectively. For the 20 mm ϕ longitudinal bars, the yield and ultimate stress were 500 and 650 MPa, respectively.

The analytical findings can be seen by reference to Fig. 19 where crack patterns at various load levels up to failure and a comparison of the analytical load-deflection curve with its experimental counterpart is given. As depicted in the Figure, the first flexural cracks occurred in the midspan and under the point load at 43.2 kN. Soon the web in the shear span was full of inclined cracks. The whole process stabilised at 115.2 kN, when a few cracks reached the bottom part of the top flange. The beam model ultimately sustained a load of 187.2 kN (i.e. 94% of the actual collapse load (200 kN)). At this MSL, vertical cracks formed in the upper half of the top flange, while the bottom steel in the flexural span actually reached yield in the previous load step. Figure 19 clearly shows the ductile behaviour of the beam, both experimentally and analytically, the two curves exhibiting good agreement, especially as

regards the stiffness of the ascending branch and the ductility of the near-horizontal branch.

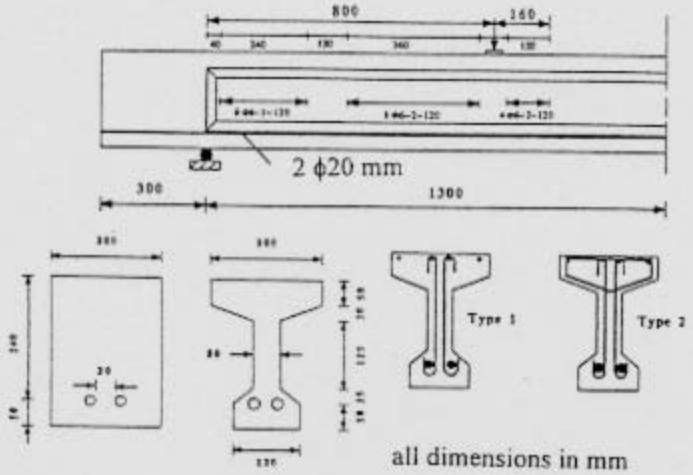

Fig. 17 Case study 5. Dimensions and reinforcement detailing

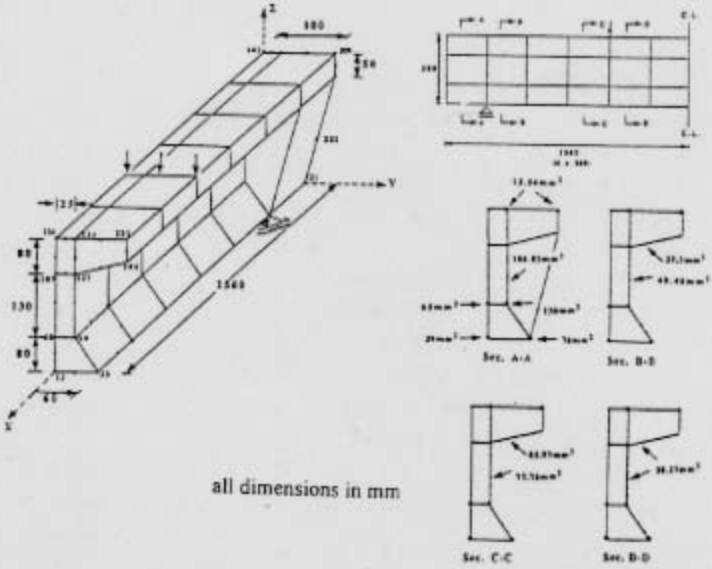

Fig. 18 Case study 5. FE mesh for one-fourth of the structure

CASE STUDY 6: RC SHEAR WALL SW11 FAILING IN FLEXURE

The last structural element considered in the present study is a RC shear wall of rectangular cross-section subjected to horizontal load, referred to as SW11 in the work of Lefas et al. (1990). The analysis of SW11 is reported in considerable detail in Gonzalez Vidosa et al. (1991c) and only the salient features of the analysis will be enumerated presently. The dimensions and reinforcement detailing, as well as the crack patterns at experimental and analytical failure are shown in Fig. 20. The specimen was made from a 44.2 MPa cylinder strength concrete. Half of the wall was discretized using 25 HX20 brick elements for concrete and 75 LM03 bar elements for steel. Results of two runs have been reported. In the first run, reinforcement was spread evenly and allowance was not made for the presence of the two concealed columns in the wall. In this case the analytical failure load underestimated the experimental value by 23%. In the second run, although no attempt was made to improve the accuracy of prediction by using a mesh finer than the initially-chosen one, denser steel distribution was allowed at the edges; this resulted in a better modelling of the concealed columns where compressive force was critical. The ensuing analysis resulted in a MSL/EXP of 0.89.

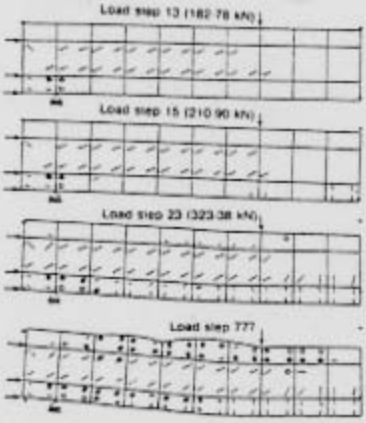

Fig. 19 Case study 5. Analytical crack patterns and comparison between experimental and analytical load-deflection curves

CONCLUSIONS

The main features of an existing "constant parameter" three-dimensional nonlinear finite element model and six case studies have been presented. The case studies include plain-, reinforced- and prestressed-concrete members. The structural members are made from both normal- and high-strength concrete. The reinforcements used in the structures ranged from mild steel to prestressing steel. The geometries of the structures and loading configurations had varying complexities as well. The actual structures were designed to both traditional- and new-concepts of structural concrete. The structural members were chosen randomly for modelling purposes and no attempt was made to get accurate predictions by mesh refinement.

It is evident from the study that the present model is capable of predicting the ultimate failure load within an approximate range of ± 10%, which is sufficient for engineering purposes. The model also predicts the failure mode well. The present model relies heavily on accurate material properties; and sensible modelling of the main geometric and reinforcement characteristics, rather than mesh refinement, seems to be the essence of reliable predictions.

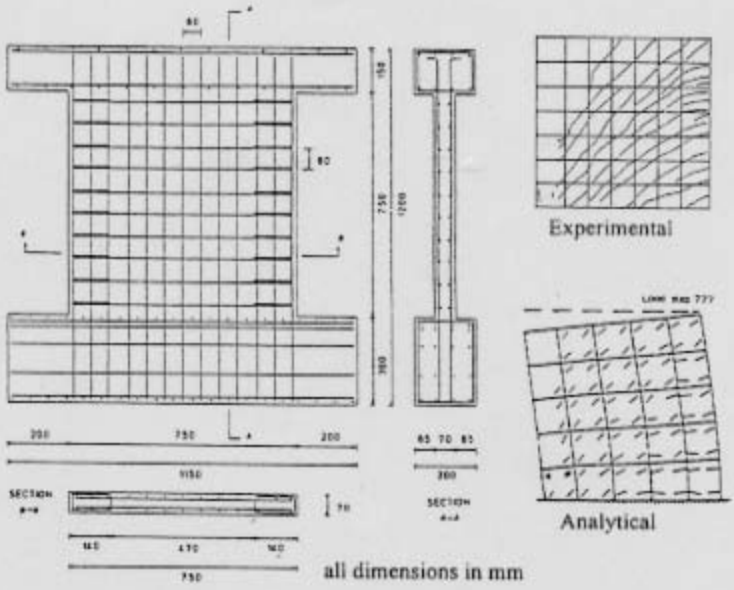

Fig. 20 Case study 6. Dimensions and reinforcement detailing, and crack patterns at failure (after Gonzalez Vidosa et al., 1991c)

REFERENCES/BIBLIOGRAPHY

Elzanaty, A. H., Nilson, A. H. and Slate, F. O., 1985
SHEAR CRITICAL HIGH STRENGTH CONCRETE BEAMS, Research Report No. 85-1, Department of Structural Engineering, Cornell University, Ithaca.

Gonzalez Vidosa, F., Kotsovos, M. D. and Pavlovic, M. N., 1988
ON THE NUMERICAL INSTABILITY OF THE SMEARED-CRACK APPROACH IN THE NON-LINEAR MODELLING OF CONCRETE STRUCTURES, Communications in Applied Numerical Methods, Vol. 4, No. 6, pp. 799-806.

Gonzalez Vidosa, F., Kotsovos, M. D. and Pavlovic, M. N., 1991a
A THREE-DIMENSIONAL NONLINEAR FINITE ELEMENT MODEL FOR STRUCTURAL CONCRETE. PART 1 : MAIN FEATURES AND OBJECTIVITY STUDY. Proc. Institution of Civil Engineers, Part 2, Vol. 91, No. 3, pp. 517-544.

Gonzalez Vidosa, F., Kotsovos, M. D. and Pavlovic, M. N., 1991b
A THREE-DIMENSIONAL NONLINEAR FINITE-ELEMENT MODEL FOR STRUCTURAL CONCRETE. PART 2 : GENERALITY STUDY. Proc. Institution of Civil Engineers, Part 2, Vol. 91, No. 3, pp. 545-560.

Gonzalez Vidosa, F., Kotsovos, M. D. and Pavlovic, M. N., 1991c
NONLINEAR FINITE-ELEMENT ANALYSIS OF CONCRETE STRUCTURES : PERFORMANCE OF A FULLY THREE-DIMENSIONAL BRITTLE MODEL. Journal of Computers & Structures, Vol. 40, No. 5, pp. 1287-1305.

Kotsovos, M. D., 1979
A MATHEMATICAL DESCRIPTION OF THE STRENGTH PROPERTIES OF CONCRETE UNDER GENERALIZED STRESS, MAGAZINE OF CONCRETE RESEARCH, Vol. 31, No. 108, pp. 151-158.

Kotsovos, M. D., 1982
A FUNDAMENTAL EXPLANATION OF THE BEHAVIOUR OF REINFORCED CONCRETE BEAMS IN FLEXURE BASED ON THE PROPERTIES OF CONCRETE UNDER MULTIAXIAL STRESS, Journal of Materials and Structures, RILEM, Vol. 15, No. 90, pp. 529-537.

Kotsovos, M. D., 1983
EFFECT OF TESTING TECHNIQUES ON THE POST-ULTIMATE BEHAVIOUR OF CONCRETE IN COMPRESSION, Journal of Materials and Structures, RILEM, Vol. 16, No. 91, pp. 3-12.

Kotsovos, M. D., 1984
Concrete. A Brittle Fracturing Material, Materials and Structures, RILEM, Vol. 17, No. 98, pp. 107-115.

Kotsovos, M. D. and Newman, J. B., 1979
A MATHEMATICAL DESCRIPTION OF THE DEFORMATIONAL BEHAVIOUR OF CONCRETE UNDER COMPLEX LOADING, MAGAZINE OF CONCRETE RESEARCH, Vol. 31, No. 107, pp. 77-90.

Kotsovos, M. D. and Newman, J. B., 1981
FRACTURE MECHANICS AND CONCRETE BEHAVIOUR, Magazine of Concrete Research, Vol. 33, No. 113, pp. 103-112.

Kotsovos, M. D. and Pavlovic, M. N., 1986
NON-LINEAR FINITE ELEMENT MODELLING OF CONCRETE STRUCTURES : BASIC ANALYSIS, PHENOMENOLOGICAL INSIGHT AND DESIGN IMPLICATIONS, Engineering Computations, Vol. 3, No. 3, pp. 243-250.

Kotsovos, M. D. and Pavlovic, M. N., 1995
STRUCTURAL CONCRETE : FINITE ELEMENT ANALYSIS FOR LIMIT-STATE DESIGN, Thomas Telford Publishers, London.

Kotsovos, M. D., Bobrowski, J and Eibl, J., 1987
BEHAVIOUR OF REINFORCED CONCRETE T-BEAMS IN SHEAR, Structural Engineers, Part B, Vol. 65, No. 1, pp. 1-10.

Lefas, I. D., Kotsovos, M. D. and Ambraseys, N. N., 1990
BEHAVIOUR OF REINFORCED CONCRETE STRUCTURAL WALLS : STRENGTH, DEFORMATION CHARACTERISTICS AND FAILURE MECHANISM, American Concrete Institute Structural Journal, Vol. 87, No. 1, pp. 23-31.

Mphonde, A. G. and Frantz, G. C., 1984
SHEAR STRENGTH OF HIGH STRENGTH CONCRETE BEAMS, Report No. CE 84-157, Department of Civil Engineering, University of Connecticut.

Neville, A. M., 1981
PROPERTIES OF CONCRETE, Longman Sc. & Tech. (3rd edn), Harlow.

Niyogi, S. K., 1974
CONCRETE BEARING STRENGTH--SUPPORT, MIX, SIZE-EFFECT, Journal of Structural Engineering Division, Proc. ASCE, Vol. 100, No. 8, pp. 1685-1702.

Rashid, Y. M., 1968
ULTIMATE STRENGTH ANALYSIS OF PRESTRESSED CONCRETE PRESSURE VESSELS, Nuclear Engineering and Design, Vol. 7, pp. 334-344.

Seraj, S. M., Kotsovos, M. D. and Pavlovic, M. N., 1992a
THREE-DIMENSIONAL FINITE-ELEMENT MODELLING OF NORMAL- AND HIGH-STRENGTH REINFORCED CONCRETE MEMBERS, WITH SPECIAL REFERENCE TO T-BEAMS, Journal of Computers and Structures, Vol. 44, No. 4, pp. 699-716.

Seraj, S. M., Kotsovos, M. D. and Pavlovic, M. N., 1992b
NONLINEAR FINITE-ELEMENT ANALYSIS OF PRESTRESSED CONCRETE MEMBERS, Journal of Structures & Buildings, Proc. Institution of Civil Engineers, Vol. 94, No. 4, pp. 403-418.

Seraj, S. M., Kotsovos, M. D. and Pavlovic, M. N., 1993a
COMPRESSIVE-FORCE PATH AND BEHAVIOUR OF PRESTRESSED CONCRETE BEAMS, Journal of Materials and Structures, RILEM, Vol. 26, No. 156, pp. 74-89.

Seraj, S. M., Kotsovos, M. D. and Pavlovic, M. N., 1993b
EXPERIMENTAL STUDY OF THE COMPRESSIVE-FORCE PATH CONCEPT IN PRESTRESSED CONCRETE BEAMS, Journal of Engineering Structures, Vol. 15, No. 6, pp. 439-451.

Seraj, S. M., Kotsovos, M. D. and Pavlovic, M. N., 1994
BEHAVIOUR OF HIGH-STRENGTH MIX REINFORCED CONCRETE BEAMS, Journal of Archives of Civil Engineering, Proc. Polish Academy of Sciences, V. 40, No. 3.

Zienkiewicz, O. C., 1977
THE FINITE ELEMENT METHOD, McGraw-Hill, London.